

## Exploring a Series of Isostructural Dodecanuclear Mixed Ni:Co Clusters: Toward the Control of Elemental Composition Using pH and Stoichiometry

Geoffrey J. T. Cooper,<sup>†</sup> Graham N. Newton,<sup>†</sup> De-Liang Long,<sup>†</sup> Paul Kögerler,<sup>\*‡</sup> Mali H. Rosnes,<sup>†</sup> Marco Keller,<sup>†</sup> and Leroy Cronin<sup>\*†</sup>

Department of Chemistry, WestCHEM, Joseph Black Building, University of Glasgow, University Avenue, Glasgow, G12 8QQ United Kingdom, and Institute of Inorganic Chemistry, RWTH Aachen University, 52074 Aachen, Germany.

Received November 16, 2008

The compositional parameter space in the formation of polynuclear clusters is probed in the synthesis of a series of dodecanuclear coordination clusters of Ni<sup>II</sup> and Co<sup>II</sup> with isostructural  $D_{3h}$ -symmetric frameworks. At the core of their construction are a carbonate template and the directing ligands *cis,trans*-1,3,5-triaminocyclohexane and acetate at contrasting pH values. The pH and stoichiometric dependence has been mapped, and analysis by electrospray mass spectrometry reveals the cluster cores in solution. In two specific cases, site-specific occupations are eluded to by analysis of the magnetic properties, and we discuss the possibility of controlling the molecular composition of mixed metal polynuclear clusters.

### Introduction

The electronic and magnetic properties of high nuclearity transition metal complexes afford them the potential to act as metalloenzyme models,<sup>1</sup> nanoscale reaction containers and catalysts,<sup>2</sup> quantum computing components,<sup>3,4</sup> and molecular magnets.<sup>5,6</sup> As such, compositional and structural control in their synthesis defines a crucial synthetic target and strategies for achieving this range from the use of multidentate organic ligands<sup>7</sup> to the controlled production of molecular sections of solid-state structures, including those of transition metal oxides.<sup>8</sup> In the majority of examples, the resulting metal architectures are derived from various archetypal condensed

substructures, such as (distorted)  $M_4L_4$  cubanes (L = O, N,...). Cubanes of this type constitute a class of discrete compounds and include complexes based on  $Ni_4O_4$  or  $Co_4O_4$  structures, which for the past four decades have been studied as precursors for metal oxide nanoparticles,<sup>9</sup> novel magnetic materials,<sup>10–15</sup> and polymerization catalysts.<sup>16</sup>  $M^{II}_4O_4$  cubanes often also act as the building blocks for higher nuclearity coordination complexes, linking together through corner, edge or face-sharing modes in clusters such as

\* To whom correspondence should be addressed. E-mail: l.cronin@chem.gla.ac.uk (L.C.), paul.koegerler@ac.rwth-aachen.de (P.K.).

<sup>†</sup> University of Glasgow.

<sup>‡</sup> RWTH Aachen University.

- (1) Holm, R. H.; Kennepohl, P.; Solomon, E. I. *Chem. Rev.* **1996**, *96*, 2239.
- (2) Yoshizawa, M.; Tamura, M.; Fujita, M. *Science* **2006**, *312*, 251.
- (3) Leuenberger, M.; Loss, N. D. *Nature* **2001**, *410*, 789.
- (4) Troiani, F.; Ghirri, A.; Affronte, M.; Carretta, S.; Santini, P.; Amoretti, G.; Piligkos, S.; Timco, G. A.; Winpenny, R. E. P. *Phys. Rev. Lett.* **2005**, *94*, 207208.
- (5) Saalfrank, R. W.; Scheure, A. R.; Bernt, I.; Heinemann, F. W.; Postnikov, A. V.; Schünemann, V.; Trautwein, A. X.; Alam, M. S.; Rupp, H.; Müller, P. *Dalton Trans.* **2006**, 2865.
- (6) Schnack, J. *Lect. Notes Phys.* **2004**, *645*, 155.
- (7) Saalfrank, R. W.; Bernt, I.; Chowdhry, M. M.; Hampel, F.; Vaughan, G. B. M. *Chem.—Eur. J.* **2001**, *7*, 2765.

- (8) Kögerler, P.; Cronin, L. *Angew. Chem., Int. Ed.* **2005**, *44*, 844.
- (9) Polarz, S.; Orlov, A. V.; van den Berg, M. W. E.; Driess, M. *Angew. Chem., Int. Ed.* **2005**, *44*, 7892.
- (10) Miyasaka, H.; Nakata, K.; Lecren, L.; Coulon, C.; Nakazawa, Y.; Fujisaki, T.; Sugiura, K.-i.; Yamashita, M.; Clerac, R. *J. Am. Chem. Soc.* **2006**, *128*, 3770.
- (11) Aromi, G.; Batsanov, A. S.; Christian, P.; Helliwell, M.; Roubeau, O.; Timco, G. A.; Winpenny, R. E. P. *Dalton Trans.* **2003**, 4466.
- (12) Murrie, M.; Teat, S. J.; Stoeckli-Evans, H.; Güdel, H. U. *Angew. Chem., Int. Ed.* **2003**, *42*, 4653.
- (13) Aromi, G.; Batsanov, A. S.; Christian, P.; Helliwell, M.; Parkin, A.; Parsons, S.; Smith, A. A.; Timco, G. A.; Winpenny, R. E. P. *Chem.—Eur. J.* **2003**, *9*, 5142.
- (14) Sieber, A.; Boskovic, C.; Bircher, R.; Waldmann, O.; Ochsenein, S. T.; Chaboussant, G.; Güdel, H. U.; Kirchner, N.; Slagereen, J.; Wernsdorfer, W.; Neels, A.; Stoeckli-Evans, H.; Janssen, S.; Juranyi, F.; Mutka, H. *Inorg. Chem.* **2005**, *44*, 4315.
- (15) Yang, E.-C.; Wernsdorfer, W.; Zakharov, L. N.; Karaki, Y.; Yamaguchi, A.; Isidro, R. M.; Lu, G.-D.; Wilson, S. A.; Rheingold, A. L.; Ishimoto, H.; Hendrickson, D. N. *Inorg. Chem.* **2006**, *45*, 529.
- (16) Lassahn, P.-G.; Lozan, V.; Timco, G. A.; Christian, P.; Janiak, C.; Winpenny, R. E. P. *J. Catal.* **2004**, *222*, 260.

{Ni<sub>7</sub>},<sup>17</sup> {Co<sub>7</sub>},<sup>18</sup> {Ni<sub>8</sub>},<sup>19</sup> {Ni<sub>10</sub>},<sup>20</sup> {Ni<sub>11</sub>},<sup>21</sup> or {Co<sub>14</sub>},<sup>12</sup> and a Ni<sub>4</sub>O<sub>4</sub> cubane motif can even be integrated into a polyoxotungstate matrix.<sup>22</sup> Systematic comparative studies of isostructural metal–ligand frameworks allow for examination of their complex magnetic properties. However, the vast majority of isostructural compounds containing Ni<sup>II</sup> and Co<sup>II</sup>,<sup>23–26</sup> some of which are based on the M<sub>4</sub>O<sub>4</sub> cubane motif, are of low nuclearity, and there are very few examples of systems exceeding 10 metal centers.<sup>27,28</sup> Correspondingly, mixed-metal isostructures (i.e., structures incorporating both Ni<sup>II</sup> and Co<sup>II</sup> centers in varying ratios that are distributed over the metal framework of a coordination cluster) can be generated. However, any prediction of site-specific occupancy can only be based upon binomial statistics because of the limitations of traditional X-ray crystallographic techniques in differentiating between such similar metal centers. We discuss herein that, within the framework of a simplified magnetochemical model, the observed magnetic properties may allow identification (despite the multiparameter nature of the problem and difficulty in fitting magnetic susceptibility data when the system has many parameters) between possible distribution scenarios in such materials<sup>29</sup> and to indicate the width of the distribution curves for (co-crystallizing) compositions (whereby the distribution for a given composition {M<sub>x</sub>M'<sub>y</sub>} exhibits a symmetrical spread from {M<sub>x-Δ</sub>M'<sub>y+Δ</sub>} to {M<sub>x+Δ</sub>M'<sub>y-Δ</sub>}) and present this work as an extension to our previous communication that presented the isostructural {Co<sub>12</sub>} and {Ni<sub>12</sub>} clusters.<sup>30</sup>

A crucial building block in the synthesis of the presented family of {M<sub>12</sub>} coordination clusters is the aliphatic triamine ligand *cis,trans*-1,3,5-triaminocyclohexane (*trans*-tach). Previous work has led to the synthesis of both discrete coordination complexes and polynuclear coordination net-

works<sup>30–35</sup> based on *trans*-tach. The *trans* version of the ligand is particularly versatile because of the rigidity of its cyclohexane backbone which prevents the interaction of all three amino donor groups with one single metal center, while reversible conformational inversion of the backbone allows *monoaxial-bisequatorial* and *bisaxial-monoequatorial* coordination modes, although the *cis* version has also been used to form interesting metal complexes.<sup>36</sup> Invariably, it is the latter conformation which is observed upon coordination to open-shell transition metal cations where the *trans*-tach ligand can simultaneously act as a *bis*-chelating ligand and as an anchor into supramolecular hydrogen-bonded networks through the easily protonated<sup>37</sup> equatorial *trans*-amine “tail” group. Previously,<sup>30</sup> we demonstrated the use of *trans*-tach, in conjunction with bridging acetate and templating carbonate ligands, to support the directed assembly of high-nuclearity {Ni<sub>12</sub>} and {Co<sub>12</sub>} clusters, each consisting of three isostructural M<sub>4</sub>O<sub>4</sub> cubane units arranged symmetrically around a central templating carbonate anion. Moreover, we present the idea that the isostructural mixed Ni:Co clusters can be accessed by controlling the pH/metal ion ratio of the reaction solution.<sup>38</sup> The pH value thus represents a complementary reaction parameter in addition to the stoichiometric reaction ratio of Ni and Co, to differentiate the relative population of the metal sites in the {M<sub>12</sub>} system. It appears that this approach may allow the isolation of intermediates of *discrete* (i.e., non-mixed) compositions {Ni<sub>12-n</sub>Co<sub>n</sub>} (*n* = 1, 2, ..., 11) which make up a series for which the resulting magnetic properties can be fine-tuned (Figure 1). In two specific examples, {Ni<sub>11</sub>Co<sub>1</sub>} (**3**) and {Ni<sub>6</sub>Co<sub>6</sub>} (**4**), the magnetic properties, again within the limits of the used model, allow us to postulate the possibility of Ni:Co specific binding sites in the given {M<sub>12</sub>} structure; in the design of new functional architectures, this site-specific resolution is a critical goal.

## Experimental Section

**Materials, Methods and Instrumentation.** The ligand *trans*-tach was synthesized from 1,3,5-triaminobenzene following literature methods.<sup>39</sup> All other reagents and solvents were purchased as AR grade and used without further purification. All complexations were performed under a stream of dry N<sub>2</sub> gas with degassed solvents. Fourier transform infrared (FT-IR) spectra were run on a

- (17) Keene, T. D.; Hursthouse, M. B.; Price, D. J. *New J. Chem.* **2004**, 28, 558.  
 (18) Chiang, R.-K.; Huang, C.-C.; Wur, C.-S. *Inorg. Chem.* **2001**, 40, 3237.  
 (19) Murrie, M.; Biner, D.; Stoeckli-Evans, H.; Güdel, H. U. *Chem. Commun.* **2003**, 230.  
 (20) Shaw, R.; Tidmarsh, I. S.; Laye, R. H.; Breeze, B.; Helliwell, M.; Brechin, E. K.; Heath, S. L.; Murrie, M.; Ochsenbein, S.; Güdel, H.-U.; McInnes, E. J. L. *Chem. Commun.* **2004**, 1418.  
 (21) Brechin, E. K.; Clegg, W.; Murrie, M.; Parsons, S.; Teat, S. J.; Winpenny, R. E. P. *J. Am. Chem. Soc.* **1998**, 120, 7365.  
 (22) Kortz, U.; Teze, A.; Herve, G. *Inorg. Chem.* **1999**, 38, 2038.  
 (23) Ayyappan, P.; Evans, O. R.; Lin, W. *Inorg. Chem.* **2001**, 40, 4627.  
 (24) Delgado, F. S.; Hernandez-Molina, M.; Sanchi, J.; Ruiz-Perez, C.; Rodriguez-Martin, Y.; Lopez, T.; Lloret, F.; Julve, M. *CrystEngComm* **2004**, 6, 106.  
 (25) Leonard, M. A.; Squattrito, P. J.; Dubey, S. N. *Acta Crystallogr. C* **1999**, C55, 35.  
 (26) Malkov, A. E.; Fomina, I. G.; Sidorov, A. A.; Aleksandrov, G. G.; Egorov, I. M.; Latosh, N. I.; Chupakhin, O. N.; Rusinov, G. L.; Rikitin, Y. V.; Novotortsev, V. M.; Ikorskii, V. N.; Eremenko, I. L.; Moiseev, I. J. *Mol. Struct.* **2003**, 656, 207.  
 (27) Blake, A. J.; Grant, C. M.; Parsons, S.; Rawson, J. M.; Winpenny, R. E. P. *Chem. Commun.* **1994**, 2363.  
 (28) Brechin, E. K.; Cador, O.; Caneschi, A.; Cadiou, C.; Harris, S. G.; Parsons, S.; Vooni, M.; Winpenny, R. E. P. *Chem. Commun.* **2002**, 1860.  
 (29) For a similar analysis of a magnetic mixed-metal framework see Müller, A.; Das, S. K.; Talismanova, M. O.; Bögge, H.; Kögerler, P.; Schmidtman, M.; Talismanov, S. S.; Luban, M.; Krickemeyer, E. *Angew. Chem., Int. Ed.* **2002**, 41, 579.  
 (30) Cooper, G. J. T.; Newton, G. N.; Kögerler, P.; Long, D.-L.; Engelhardt, L.; Luban, M.; Cronin, L. *Angew. Chem., Int. Ed.* **2007**, 46, 1340.

- (31) Seeber, G.; Kögerler, P.; Kariuki, B. M.; Cronin, L. *Chem. Commun.* **2004**, 1580.  
 (32) Schnack, J.; Nojiri, H.; Kögerler, P.; Cooper, G. J. T.; Cronin, L. *Phys. Rev. B* **2004**, 70, 174420/1–5.  
 (33) Pickering, A. L.; Seeber, G.; Long, D.-L.; Cronin, L. *Chem. Commun.* **2004**, 136.  
 (34) Seeber, G.; Pickering, A. L.; Long, D.-L.; Cronin, L. *Chem. Commun.* **2003**, 2002.  
 (35) Seeber, G.; Kariuki, B.; Cronin, L. *Chem. Commun.* **2002**, 2912.  
 (36) Boxwell, C. J.; Bhalla, R.; Cronin, L.; Turner, S. S.; Walton, P. H. *Dalton Trans.* **1998**, 2449.  
 (37) Although the measured p*K<sub>a</sub>* values are very similar for the three amines, the chelating coordination of a metal ion at the *cis*-amine positions leads to coordinative speciation and favors protonation of the *trans*-amine.  
 (38) Note that we refer to measuring the apparent pH value in methanolic solutions with a minimal water content; therefore, our pH measurements should not be related to measurements in water without considering that the hydrogen ion activity is not referred to in the standard state, p<sub>a</sub>H but rather now to p<sub>a</sub>H\* in methanol.  
 (39) Lions, F.; Martin, K. V. *J. Am. Chem. Soc.* **1957**, 79, 1572.

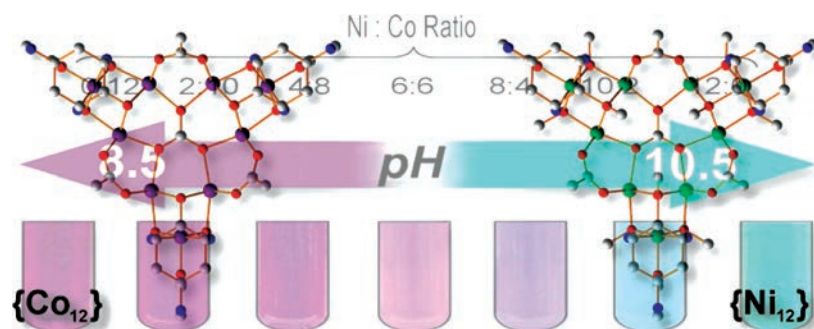


**Figure 1.** Structures of the  $\{\text{Co}_{12}\}$  **1** and  $\{\text{Ni}_{12}\}$  **2** complexes, and a schematic showing the colors of mixed  $\{\text{Ni}_{12-n}\text{Co}_n\}$  ( $n = 1, 2, \dots, 11$ ) intermediates. Ni: green, Co: purple, C: gray, N: blue, O: red.

JASCO FTIR 410 spectrometer. UV–visible spectra were collected on a Shimadzu UV-3101PC spectrometer. Details of X-ray diffraction experiments are included in the crystallographic data section. Magnetic susceptibility data were recorded for 2–290 K using a Quantum Design MPMS-5 SQUID magnetometer. Mass spectra were collected using a Bruker microTOFQ spectrometer with the Cryospray attachment.

**Preparation of  $[\text{Co}_{12}(\text{trans-tachH})_6(\text{OH})_9(\text{OMe})_3(\text{OAc})_9(\text{CO}_3)](\text{ClO}_4)_7 \cdot 12 \text{ MeOH}$  (**1**).** Dilute perchloric acid (13% in water) was used to acidify a solution of *trans-tach* (0.050 g, 0.388 mmol) in methanol (5 mL) to pH 8.5 which was subsequently degassed by bubbling with dry nitrogen gas. Addition of cobalt(II) acetate tetrahydrate (0.096 g, 0.388 mmol) and sodium carbonate (0.003 g, 0.032 mmol) to this solution gave a dark purple solution which was stirred for a few minutes under a nitrogen atmosphere and then filtered through glass fiber paper. Hexagonal, dark red diffraction quality crystals of **1** were obtained in a yield of 11.0% (25 mg, 0.0073 mmol) by the slow diffusion of ether into this solution over 3 to 5 days. Data for **1**:  $T_{\text{decomp.}} = 290$  °C; FT-IR (KBr)  $\nu/\text{cm}^{-1}$  3420–3000(s), 2088(m), 1558(s), 1408(s), 1264(w), 1159(w), 1020(m), 932(w), 790(w), 667(m); UV/vis (MeOH, 293 K)  $\epsilon$ : 640  $\text{mol}^{-1} \text{ dm}^3 \text{ cm}^{-1}$  (530 nm); elemental analysis calcd for  $\text{C}_{70}\text{H}_{189}\text{Co}_{12}\text{Cl}_7\text{N}_{18}\text{O}_{73}$ : C 24.68, H 5.59, N 7.40%; found: C 24.60, H 5.00, N 7.40%; thermogravimetric analysis (TGA) shows a mass reduction of 10% upon heating to 200 °C; unit cell parameters: Hexagonal,  $a = 21.3178(5)$ ,  $c = 23.3757(6)$  Å.

**Preparation of  $[\text{Ni}_{12}(\text{trans-tachH})_6(\text{OMe})_{12}(\text{OAc})_9(\text{CO}_3)](\text{OAc})_7 \cdot 10 \text{ MeOH} \cdot 6\text{H}_2\text{O}$  (**2**).** Addition of nickel(II) acetate tetrahydrate (0.095 g, 0.388 mmol) and sodium carbonate (0.003 g, 0.032 mmol) to a solution of *trans-tach* (0.050 g, 0.388 mmol) in methanol (5 mL) gave a light green solution of pH 10.5 which was stirred for 1 h and then filtered through glass fiber paper. Slow diffusion of ether into this solution over 3 days gave green diffraction quality crystals of **2** in a yield of 14.0% (29 mg, 0.0088 mmol). Data for **2**:  $T_{\text{decomp.}} = 290$  °C; FT-IR (KBr)  $\nu/\text{cm}^{-1}$  3316(s), 2175(w), 1560(s), 1164(w), 1048(m), 918(m), 670(m); UV/vis (MeOH, 293 K)  $\epsilon$ : 211  $\text{mol}^{-1} \text{ dm}^3 \text{ cm}^{-1}$  (386 nm), 119  $\text{mol}^{-1} \text{ dm}^3 \text{ cm}^{-1}$  (656 nm); elemental analysis calcd for  $\text{C}_{81}\text{H}_{192}\text{Ni}_{12}\text{N}_{18}\text{O}_{53}$  (10 MeOH lost in drying, see below): C 32.75, H 6.52, N 8.49%; found: C 32.10, H 7.00, N 9.00%. TGA analysis shows a mass reduction of 14% upon heating to 200 °C; Unit cell parameters: Orthorhombic,  $a = 19.8251(7)$ ,  $b = 38.3999(13)$ ,  $c = 23.6258(7)$  Å.

**Preparation of  $[\text{Ni}_1\text{Co}_9(\text{trans-tachH})_6(\text{OMe})_{12}(\text{OAc})_9(\text{CO}_3)](\text{OAc})_7 \cdot 10 \text{ MeOH} \cdot 6\text{H}_2\text{O}$  (**3**).** Dilute acetic acid (11% in water) was used to acidify a solution of *trans-tach* (0.050 g, 0.388 mmol) in methanol (5 mL) to pH 10.2 which was subsequently degassed by bubbling with dry nitrogen gas. Addition of nickel(II) acetate tetrahydrate (0.087 g, 0.356 mmol), cobalt(II) acetate tetrahydrate (0.008 g, 0.032 mmol), and sodium carbonate (0.003 g, 0.032 mmol) resulted in a

**Table 1.** Reagent Quantities and pH Conditions for the Preparation of **5–8**

code	Ni/Co	$\text{Co}(\text{OAc})_2 \cdot 4\text{H}_2\text{O}$	$\text{Ni}(\text{OAc})_2 \cdot 4\text{H}_2\text{O}$	pH
<b>5</b>	10:2	0.032 g, 0.129 mmol	0.160 g, 0.647 mmol	10.10
<b>6</b>	8:4	0.048 g, 0.194 mmol	0.114 g, 0.582 mmol	9.80
<b>7</b>	4:8	0.064 g, 0.259 mmol	0.128 g, 0.517 mmol	9.20
<b>8</b>	2:10	0.128 g, 0.517 mmol	0.064 g, 0.259 mmol	8.90

light blue-green solution which was stirred for 1 h under nitrogen and then filtered through glass fiber paper. Slow diffusion of ether into this solution over 3 days gave blue-green diffraction quality crystals of **3** in a yield of 12.7% (23 mg, 0.0082 mmol). Data for **3**: FT-IR (KBr)  $\nu/\text{cm}^{-1}$  3446.2(vs), 2945.5(m), 2360.4(s), 2340.2(s), 1652.7(s), 1558.2(s), 1418.4(m), 1049.1(m), 668.2(m); UV/vis (MeOH, 293 K)  $\epsilon$ : 190  $\text{mol}^{-1} \text{ dm}^3 \text{ cm}^{-1}$  (377 nm), 30  $\text{mol}^{-1} \text{ dm}^3 \text{ cm}^{-1}$  (658 nm); TGA analysis shows a mass reduction of 24% upon heating to 200 °C. FAAS ppm Co 0.22, Ni 1.87, ratio Co:Ni = 1.26:10.74; Unit cell parameters: Orthorhombic,  $a = 21.53$ ,  $b = 37.29$ ,  $c = 22.78$  Å.

**Preparation of  $[\text{Ni}_6\text{Co}_6(\text{trans-tachH})_6(\text{OMe})_{12}(\text{OAc})_9(\text{CO}_3)](\text{OAc})_7 \cdot 10 \text{ MeOH} \cdot 6\text{H}_2\text{O}$  (**4**).** Dilute acetic acid (11% in water) was used to acidify a solution of *trans-tach* (0.050 g, 0.388 mmol) in methanol (5 mL) to pH 9.5 which was subsequently degassed by bubbling with dry nitrogen gas. Addition of nickel(II) acetate tetrahydrate (0.047 g, 0.194 mmol), cobalt(II) acetate tetrahydrate (0.048 g, 0.194 mmol), and sodium carbonate (0.003 g, 0.032 mmol) resulted in a pink solution which was stirred for 1 h under nitrogen and then filtered through glass fiber paper. Slow diffusion of ether into this solution over 3 days gave light red diffraction quality crystals of **4** in a yield of 11.6% (21 mg, 0.0075 mmol). Data for **4**: FT-IR (KBr)  $\nu/\text{cm}^{-1}$  3434.6(vs), 2926.5(m), 1615.1(s), 1568.8(s), 1404.9(s), 1340.3(m), 1163.8(m), 1022.1(m), 920.9(m), 661.5(m); UV/vis (MeOH, 293 K)  $\epsilon$ : 172  $\text{mol}^{-1} \text{ dm}^3 \text{ cm}^{-1}$  (540 nm); TGA analysis shows a mass reduction of 12% upon heating to 200 °C; FAAS ppm Co 0.89, Ni 0.91, ratio Co:Ni = 1.00:1.02; Unit cell parameters: Orthorhombic,  $a = 19.82$ ,  $b = 37.84$ ,  $c = 23.83$  Å.

**Preparation of Other Mixed Ni:Co  $\{\text{M}_{12}\}$  Materials (**5–8**).** A mixture of nickel(II) acetate tetrahydrate and cobalt(II) acetate tetrahydrate was added to a solution of *trans-tach* (0.100 g, 0.776 mmol) in methanol (5 mL) to which dilute acetic acid (11% in water) had previously been added to give the required pH value and which had then been degassed by bubbling of dry nitrogen gas. Slow diffusion of ether into these solutions over 3 to 5 days gave crystalline material suitable for analysis. The amounts of reagents and the pH values can be found in Table 1.

Data for **5**:  $\text{C}_{79.5}\text{H}_{189}\text{Co}_2\text{Ni}_{10}\text{N}_{18}\text{O}_{53}$  (2950.23  $\text{g mol}^{-1}$ ); relative Co/Ni actual (expected) 2.43:9.57 (2:10); FT-IR (KBr)  $\nu/\text{cm}^{-1}$  3431.7(vs), 2925.5(m), 2360.4(m), 1617.9(s), 1566.9(s), 1404.9(s), 1339.3(m), 1163.8(m), 1049.1(m), 919.9(m), 667.3(m); UV–vis ( $\text{H}_2\text{O}$ ),  $\lambda_{\text{max}}/\text{nm}$  (Abs): 456 (0.02, shoulder), 622 (0.04).

**Table 2.** Crystallographic Data for **1** and **2**<sup>a</sup>

	<b>1</b>	<b>2</b>
empirical formula	C <sub>70</sub> H <sub>189</sub> Cl <sub>7</sub> Co <sub>12</sub> Ni <sub>18</sub> O <sub>73</sub>	C <sub>91</sub> H <sub>232</sub> Ni <sub>12</sub> Ni <sub>18</sub> O <sub>63</sub>
Fw (g mol <sup>-1</sup> )	3406.70	3291.47
crystal system	hexagonal	orthorhombic
<i>a</i> (Å)	21.3178(5)	19.8251(7)
<i>b</i> (Å)	21.3178(5)	38.3999(13)
<i>c</i> (Å)	23.3757(6)	23.6258(7)
$\alpha$ (deg)	90	90
$\beta$ (deg)	90	90
$\gamma$ (deg)	120	90
space group	<i>P</i> 6 <sub>3</sub> / <i>mmc</i>	<i>Cmcm</i>
<i>V</i> (Å <sup>3</sup> )	9199.8(4)	17985.9(10)
<i>Z</i>	2	4
$\rho_{\text{calcd}}$ (g cm <sup>-3</sup> )	1.230	1.216
$\mu$ (mm <sup>-1</sup> )	1.229	1.299
<i>T</i> (K)	150(2)	150(2)
no. observations (unique)	23815	53424

<sup>a</sup> CCDC entries 620127 and 620128.<sup>30</sup>

Data for **6**: C<sub>78</sub>H<sub>186</sub>Co<sub>4</sub>Ni<sub>8</sub>Ni<sub>18</sub>O<sub>53</sub> (2929.67 g mol<sup>-1</sup>): relative Co/Ni actual (expected) 4.18:7.82 (4:8); FT-IR (KBr)  $\nu$ /cm<sup>-1</sup> 3433.6(vs), 2924.5(w), 2360.4(w), 1615.1(s), 1567.8(s), 1405.9(s), 1339.3(m), 1163.8(w), 1046.19(w), 920.8(m), 662.4(m); UV-vis (H<sub>2</sub>O),  $\lambda_{\text{max}}$ /nm (Abs): 451 (0.01, shoulder), 619 (0.06).

Data for **7**: C<sub>75</sub>H<sub>180</sub>Co<sub>8</sub>Ni<sub>4</sub>Ni<sub>18</sub>O<sub>53</sub> (2888.56 g mol<sup>-1</sup>): relative Co/Ni actual (expected) 8.70: 3.30 (8: 4); Hexagonal; 21.46, 21.46, 23.38, 90, 90, 120; FT-IR (KBr)  $\nu$ /cm<sup>-1</sup> 3435.6(vs), 2924.5(w), 1614.1(s), 1565.4(s), 1405.9(s), 1163.8(m), 1022.1(m), 920.8(m), 659.5(w); Unit cell parameters: Hexagonal, *a* = 21.46, *c* = 23.38 Å.

Data for **8**: C<sub>73.5</sub>H<sub>177</sub>Co<sub>10</sub>Ni<sub>2</sub>Ni<sub>18</sub>O<sub>53</sub> (2868.02 g mol<sup>-1</sup>): relative Co:Ni actual (expected) 9.78: 2.22 (10: 2); FT-IR (KBr)  $\nu$ /cm<sup>-1</sup> 3435.6(vs), 2924.5(w), 1612.2(s), 1405.9(s), 1020.2(m), 660.5(w).

**Single-Crystal Structure Determination.** Suitable single crystals of **1** and **2** were selected and mounted onto the end of a thin glass fiber using Fomblin oil. X-ray diffraction intensity data were measured at 150(2) K on a Nonius Kappa-CCD diffractometer [ $\lambda$ (Mo K $\alpha$ ) = 0.7107 Å]. Structure solution and refinement was carried out with SHELXS-97<sup>40</sup> and SHELXL-97<sup>41</sup> using WinGX.<sup>42</sup> Corrections for incident and diffracted beam absorption effects were applied using empirical<sup>43</sup> or numerical methods.<sup>44</sup> **1**: C<sub>70</sub>H<sub>189</sub>Cl<sub>7</sub>Co<sub>12</sub>Ni<sub>18</sub>O<sub>73</sub>, *M*<sub>r</sub> = 3406.70 g mol<sup>-1</sup>; block crystal: 0.34 × 0.30 × 0.22 mm<sup>3</sup>; *T* = 150(2) K. Hexagonal, space group *P*6<sub>3</sub>/*mmc*, *a* = 21.3178(5), *c* = 23.3757(6) Å, *V* = 9199.8(4) Å<sup>3</sup>, *Z* = 2,  $\rho$  = 1.230 g cm<sup>-3</sup>,  $\mu$ (MoK $\alpha$ ) = 1.228 mm<sup>-1</sup>, *F*(000) = 3524, 23815 reflections measured, of which 2806 are independent (*R*<sub>int</sub> = 0.046), 215 refined parameters, *R*1 = 0.087, *wR*2 = 0.278. **2**: C<sub>91</sub>H<sub>232</sub>Ni<sub>12</sub>Ni<sub>18</sub>O<sub>63</sub>, *M*<sub>r</sub> = 3291.47 g mol<sup>-1</sup>; block crystal: 0.20 × 0.20 × 0.15 mm<sup>3</sup>; *T* = 150(2) K. Orthorhombic, space group *Cmcm*, *a* = 19.8251(7), *b* = 38.3999(13), *c* = 23.6258(7) Å, *V* = 17985.9(10) Å<sup>3</sup>, *Z* = 4,  $\rho$  = 1.216 g cm<sup>-3</sup>,  $\mu$ (MoK $\alpha$ ) = 1.299 mm<sup>-1</sup>, *F*(000) = 6976, 53424 reflections measured, of which 6647 are independent (*R*<sub>int</sub> = 0.1259), 215 refined parameters, *R*1 = 0.073, *wR*2 = 0.232 (Table 2).

**Magnetic Data.** Susceptibility measurements were performed for 0.1–5.0 T and 2–290 K using a Quantum Design MPMS-5 SQUID magnetometer. All susceptibility data have been corrected for calculated diamagnetic contributions. Heisenberg exchange-type

spin Hamiltonians were of the form  $H = -JS_i \cdot S_j$  (for the interaction of spin centers *i* and *j*). Importantly preliminary low-temperature (0.4 K) measurements for both compounds **1** and **2** of the magnetization as a function of the magnetic field reveal strong anisotropy that effectively erodes expected spin-level crossings caused by the intersecting Zeeman-split multiplet states in the magnetic excitation spectrum. This also exemplifies the limits of the employed isotropic Heisenberg models that are used to study the susceptibility versus temperature graphs resulting for potential distribution scenarios in mixed-metal {Ni<sub>12-n</sub>Co<sub>n</sub>} species, necessitated by the high spin nuclearities, complex exchange pathways, and plethora of anisotropy and zero-field-splitting effects present in these structures. Note that these simulations do not account for ligand-field splitting and spin-orbit coupling effects that are known to be significant for both Ni(II) and Co(II) centers in octahedral fields; therefore, the results are discussed in a purely comparative context.

**Mass Spectrometry.** Cryospray/Electrospray mass spectrometric measurements were carried out with the sprayer gas at -40 °C and the dry gas at -20 °C: These experiments were carried out at concentrations of the complex in the region of 10<sup>-5</sup> mol L<sup>-1</sup> in methanol using a Bruker microTOFQ instrument. Data was collected in positive ion mode, and the spectrometer was previously calibrated with the standard tune mix to give a precision of about 1.5 ppm in the region of 500–3000 *m/z*. The standard parameters for a medium mass data acquisition were used, the end plate voltage was set to -500 V, and the capillary to +4500 V.

## Results and Discussion

The {Co<sub>12</sub>} cluster, **1**, is prepared by addition of cobalt(II) acetate to a methanolic solution of *trans*-tach in a 1:1 molar ratio with sufficient addition of dilute perchloric (or acetic) acid to achieve pH 8.5, resulting in a purple solution from which crystals of [Co<sup>II</sup><sub>12</sub>(*trans*-tachH)<sub>6</sub>(OH)<sub>9</sub>(OMe)<sub>3</sub>(OAc)<sub>9</sub>(CO<sub>3</sub>)](ClO<sub>4</sub>)<sub>7</sub>·12 MeOH (**1**) are isolated. The analogous reaction of nickel(II) acetate with *trans*-tach in methanol at an unadjusted pH of 10.5 yields a green solution from which crystals of [Ni<sup>II</sup><sub>12</sub>(*trans*-tachH)<sub>6</sub>(OMe)<sub>12</sub>(OAc)<sub>9</sub>(CO<sub>3</sub>)](OAc)<sub>7</sub>·10 MeOH·6 H<sub>2</sub>O (**2**) can be grown. Furthermore, the cluster cores of {Co<sub>12</sub>} = [Co<sub>12</sub>(*trans*-tachH)<sub>6</sub>(OH)<sub>9</sub>(OMe)<sub>3</sub>(OAc)<sub>9</sub>(CO<sub>3</sub>)]<sup>7+</sup> (**1a**) and {Ni<sub>12</sub>} = [Ni<sub>12</sub>(*trans*-tachH)<sub>6</sub>(OMe)<sub>12</sub>(OAc)<sub>9</sub>(CO<sub>3</sub>)]<sup>7+</sup> (**2a**) differ only in the relative amounts of  $\mu_3$ -hydroxo and  $\mu_3$ -methoxo groups found in the cubane units but show striking differences in the long-range ordering of clusters in the crystalline state; this is partly caused by the interactions between the protonated *trans*-amino groups in *trans*-tach between adjacent clusters in the crystal lattice; this is also a clear example of where weaker non-covalent interactions are used to successfully direct the formation of the cluster superstructures. The formation of both **1** and **2** is controlled by the availability of carbonate anions, and a small addition of a carbonate source reduces the crystallization time from weeks to days, especially in the case of {Co<sub>12</sub>}, where other templates may take the place of carbonate at lower pH.<sup>45</sup> In both **1** and **2**, the cluster frameworks are of *D*<sub>3h</sub> symmetry and comprise a central planar carbonate dianion which bridges the faces of three

(40) Sheldrick, G. M. *Acta Crystallogr., Sect. A* **1998**, *A46*, 467.

(41) Sheldrick, G. M. *SHELXL-97. Program for Crystal structure analysis*; University of Göttingen: Göttingen, Germany, 1997.

(42) Farrugia, L. J. *J. Appl. Crystallogr.* **1999**, *32*, 837.

(43) Blessing, R. H. *Acta Crystallogr., Sect. A* **1995**, *51*, 33.

(44) Coppens, P.; Leiserowitz, L.; Rabinovich, D. *Acta Crystallogr.* **1965**, *18*, 1035.

(45) Newton, G. N.; Cooper, G. J. T.; Kögerler, P.; Long, D.-L.; Cronin, L. *J. Am. Chem. Soc.* **2008**, *130*, 790–791.

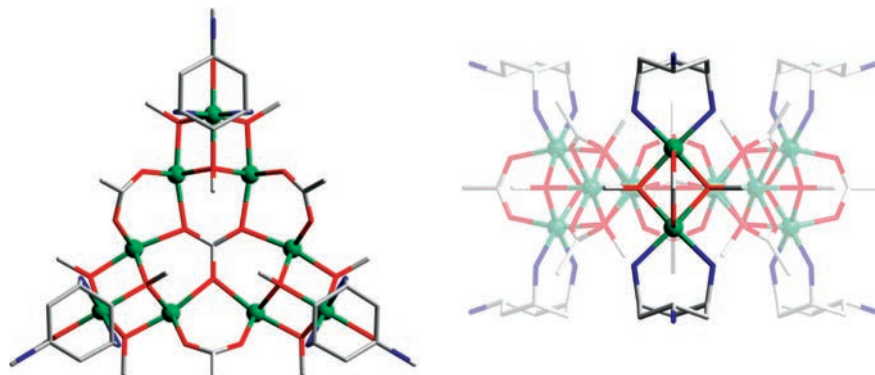


**Figure 2.** Structure of the  $\{Ni_{12}\}$  complex **2a** along the  $C_3$  axis (left) and one of the three  $C_2$  axes (right). Ni: green, C: gray, N: blue, O: red.

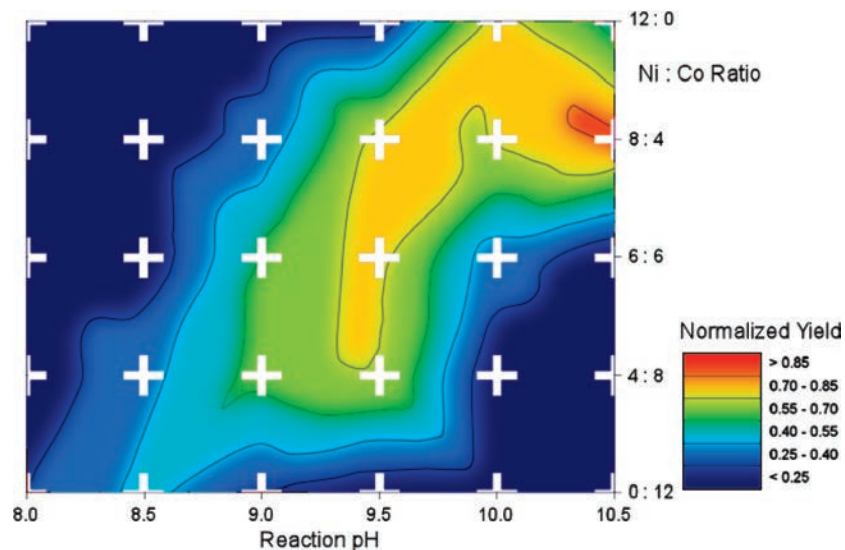


**Figure 3.**  $\{M_{12}\}$  reaction yield optimization map, showing a normalized experimental yield plotted against the starting pH and the Ni:Co ratio. 40 crystallizations were performed to generate each data point (represented by white crosses). See Experimental Section for raw data.

distorted  $\{M_4(OR)_4\}$  cubanes ( $R = CH_3$  or  $H$ ), generating an inner planar  $M_6$  ring. In **1a**, the oxygen vertices of each cubane belong to both methoxy and hydroxy ligands which are disordered in a ratio of 1:3 with methoxy ligands only being found on the outer-face positions, while in **2a** the cubanes contain only methoxy ligands (Figure 2).

The pH difference of 2.0 that is necessary for optimal formation and isolation of the pure  $\{Co_{12}\}$  and  $\{Ni_{12}\}$  cluster species becomes a critical reaction control parameter in the generation of mixed  $\{Ni_{12-n}Co_n\}$  clusters with a discrete value of  $n$ . In the absence of such a differentiating factor the similarity between  $Co^{II}$  and  $Ni^{II}$  we suggest this would cause the formation and co-crystallization of a certain range of compositions (i.e., a range of values for  $n$ ) even if the reaction educts are dosed to meet a specified stoichiometric Ni:Co ratio. However, by using this relationship, it appears to have been possible to produce all the elements ( $n = 1-11$ ) in the series; this is according to bulk analysis and does not give information about the composition of individual cluster units. It was initially observed that the species with high  $Co^{II}$  content were only produced when the pH was adjusted to around 8.0–8.5, whereas for the more  $Ni^{II}$  rich species, chain-like architectures were observed<sup>46</sup> in this range and the desired  $\{M_{12}\}$  was only observed above pH 9.0. Further

analysis of the crystallization yields over a range of pH values and stoichiometries has allowed the generation of a yield map, plotted as function of Ni:Co ratio against pH (8.0–10.5). Preliminary data demonstrate that the maximum yield is only generated at the precise pH and Ni:Co ratio as projected by a linear interpolation between pure  $\{Co_{12}\}$  at pH 8.5 and pure  $\{Ni_{12}\}$  at pH 10.5 (Figure 3). Flame atomic absorption studies on the series of  $\{Ni_{12-n}Co_n\}$  clusters showed that the Ni:Co ratio of the starting materials was maintained in the final crystalline products. However, further analysis was needed to determine if these materials really contained mixed clusters of a single composition.

The cubane subunits of both **1** and **2** are linked to one another by bridging coordination of the inner-face metal centers of neighboring cubane units: by the central templating carbonate anion and by two acetate ligands (Figure 2). The coordination spheres of the metal centers at the outer-face vertices of each cubane are completed by a bridging acetate ligand (oriented vertically) and two *trans*-tach ligands binding in the expected *bisaxial-monoequatorial* conformation through the two *cis*-amine N positions. The uncoordinated *trans*-amine groups are protonated and thus hydrogen bonding sites and unavailable for metal complexation, rendering the

(46) Newton, G. N.; Cooper, G. J. T.; Long, D.-L.; Kögerler, P.; Cronin, L. *J. Mol. Struct.* **2006**, *796*, 23.

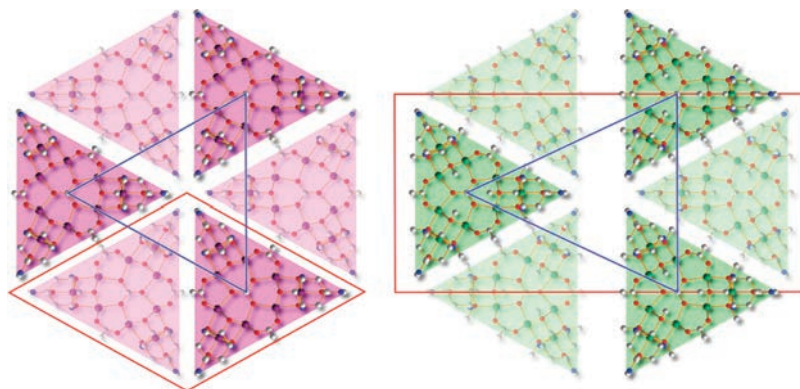


**Figure 4.** Comparison of the packing of  $\{\text{Ni}_{12}\}$  clusters in **1** (left, hexagonal system) and **2** (right, orthorhombic system) within the crystallographic  $ab$  plane. Red lines show the unit cell boundaries, and blue triangles are used to highlight the geometrical relationship enforced by hydrogen bonding between adjacent clusters.

**Table 3.** Crystallographic Unit Cell Data for **1–4** and **7**

	Ni:Co	crystal system	$a$ (Å)	$b$ (Å)	$c$ (Å)
<b>2</b>	12:0	orthorhombic	19.83	38.40	23.63
<b>3</b>	11:1	orthorhombic	21.53	37.29	22.78
<b>4</b>	6:6	orthorhombic	19.82	37.84	23.83
<b>7</b>	4:8	hexagonal	21.46	21.46	23.38
<b>1</b>	0:12	hexagonal	21.32	21.32	23.38

sterically demanding *trans*-tach unit a terminating group. The geometry of the  $\{\text{Ni}_{12}\}$  and  $\{\text{Co}_{12}\}$  clusters is nearly identical with the cubanes of **2a** being very slightly compressed compared to those in **1a**, leading to a greater separation of the cubanes as the geometry of the central carbonate anion remains constant.

Despite the isostructural nature of the cluster core frameworks, the crystal packing of **1** and **2** is significantly different. Hydrogen bonds between the protonated *trans*-amine groups and acetate counterions connect neighboring cluster units. In **1**, the hydroxyl ligands in the outer-face cubane vertices also form hydrogen bonds with solvent molecules, which is not possible in **2**. This leads to a hexagonal crystal system for **1** where the closest *trans*-tach ligands of any three adjacent clusters describe an equilateral triangle while an orthorhombic system is observed for **2** with these *trans*-tach ligands describing isosceles triangles (Figure 4). Therefore, the compositional mapping from  $\{\text{Co}_{12}\}$  to  $\{\text{Ni}_{12}\}$  structure types can be monitored crystallographically in the following manner:  $\{\text{Co}_{12}\}$  (**1**) to  $\{\text{Co}_8\text{Ni}_4\}$  (**7**)—hexagonal,  $\{\text{Ni}_{12}\}$  (**2**) to  $\{\text{Ni}_6\text{Co}_6\}$  (**4**)—orthorhombic (Table 3). This phenomenon arises through the relative affinity toward hydroxide or methoxide ligands of  $\text{Co}^{\text{II}}$  and  $\text{Ni}^{\text{II}}$  ions and their preferential occupation of inner or outer cubane sites (as discussed later with magnetism arguments).

Low-field magnetic susceptibility data for 2–290 K of **2** shows features of both antiferromagnetic and ferromagnetic exchange coupling between the  $s = 1$   $\text{Ni}^{\text{II}}$  centers, resulting in a maximum of  $\chi T$  at 27 K (Figure 5). While low-temperature high-field magnetization measurements clearly indicate anisotropic contributions due to the spin–orbit coupling of the  $\text{Ni}^{\text{II}}$  centers, we were able to reproduce the temperature dependence of the magnetic susceptibility of **2** within an isotropic Heisenberg model (see Experimental Section) that, based on the  $D_{3h}$  symmetry of **2a**, adopts four coupling constants (see inset Figure 5):  $J_1$  (red), between

adjacent Ni positions of neighboring  $\text{Ni}_4\text{O}_4$  cubanes (inter-cubane, mediated by the carbonate and two acetate bridges);  $J_2$  (blue), between the two inner-face Ni positions (two oxo and one carbonate bridges);  $J_3$  (yellow), between inner-face and outer-face Ni positions (one oxo and one methoxy bridge per Ni–Ni contact);  $J_4$  (green), between the two outer-face Ni centers (two methoxy and one acetate bridge). Because of the complexity of this system with a Hilbert space dimension of  $3^{12}$  quantum Monte Carlo simulations<sup>47,48</sup> were performed to scan the parameter space  $J_{1-4}$  and  $g$ , and the best fit resulted for antiferromagnetic inter-cubane ( $J_1/k_B = -17.5$  K) and ferromagnetic intra-cubane with strong variations of the individual exchange strengths, reflecting ferro/antiferromagnetic competition between the involved exchange pathways ( $J_2/k_B = 9.5$  K,  $J_3/k_B = 1.9$  K,  $J_4/k_B = 22.0$  K) and these studies were reported previously by us in ref 30, but also help us in our analysis here. The (isotropic)  $g$  factor was determined to 2.21, a typical value for a  $\text{Ni}^{\text{II}}$  center in an octahedral ligand field. Whereas the corresponding  $\chi T$  versus  $T$  graph for the  $s = 3/2$   $\text{Co}^{\text{II}}$  derivative **1** does not exhibit a maximum and continually decreases toward lower temperatures, we suspect that the intramolecular coupling is very similar to that established for **2**<sup>49</sup> but is masked by dominating single-ion anisotropy zero-field splitting (ZFS) contributions typical for  $s = 3/2$   $\text{Co}^{\text{II}}$  in octahedral ligand fields.

The magnetic susceptibility data for the mixed  $\{\text{Ni}_{12-n}\text{Co}_n\}$  clusters, plotted as  $\chi T$  against  $T$ , clearly shows the gradual change in character as the  $\text{Co}^{\text{II}}$  content increases and the contribution from single-ion anisotropy ZFS becomes more apparent (Figure 5). For the  $\text{Co}^{\text{II}}$  rich materials **1**, **4**, **7**, and **8**, this effect masks the ferromagnetic intra-cubane exchange while it can be seen in the  $\text{Ni}^{\text{II}}$  rich materials **2**, **3**, **5**, and **6**. This change also correlates with the observed switch in the crystal system from the unit cell data which is caused by the increasing occupation of the cubane vertices by hydroxide anions allowing the intermolecular hydrogen bonding interactions which stabilize the hexagonal system.

(47) Syljuasen, O.; Sandvik, A. *Phys. Rev. E* **2002**, *66*, 046701.

(48) Engelhardt, L.; Luban, M. *Phys. Rev. B* **2006**, *73*, 054430.

(49) Bossek, U.; Nühlen, D.; Bill, E.; Glaser, T.; Krebs, C.; Weyhermüller, T.; Wieghardt, K.; Lengen, M.; Trautwein, A. X. *Inorg. Chem.* **1997**, *36*, 2834.

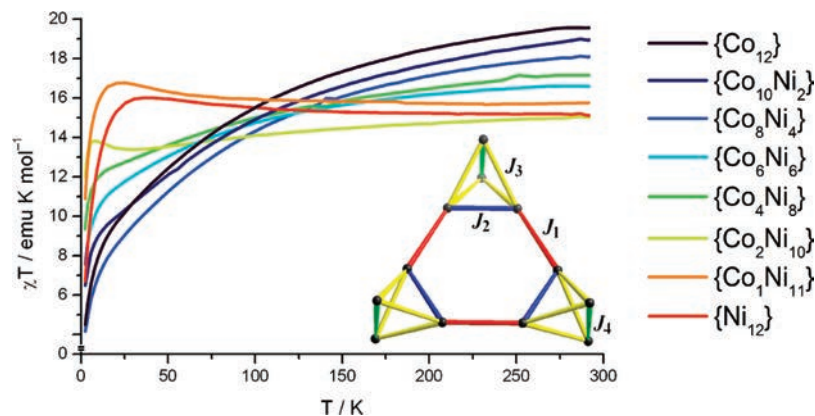


**Figure 5.** Magnetic susceptibility data for the  $\{\text{Ni}_{12-n}\text{Co}_n\}$  series of  $\{\text{M}_{12}\}$  clusters presented as plots of  $\chi T$  against  $T$  measured between 2 and 290 K in a 0.1 T field. Inset: Assignment of the exchange parameters  $J_{1-4}$  to the  $\{\text{M}_{12}\}$  spin array:  $J_1$ : red,  $J_2$ : blue,  $J_3$ : yellow,  $J_4$ : green.

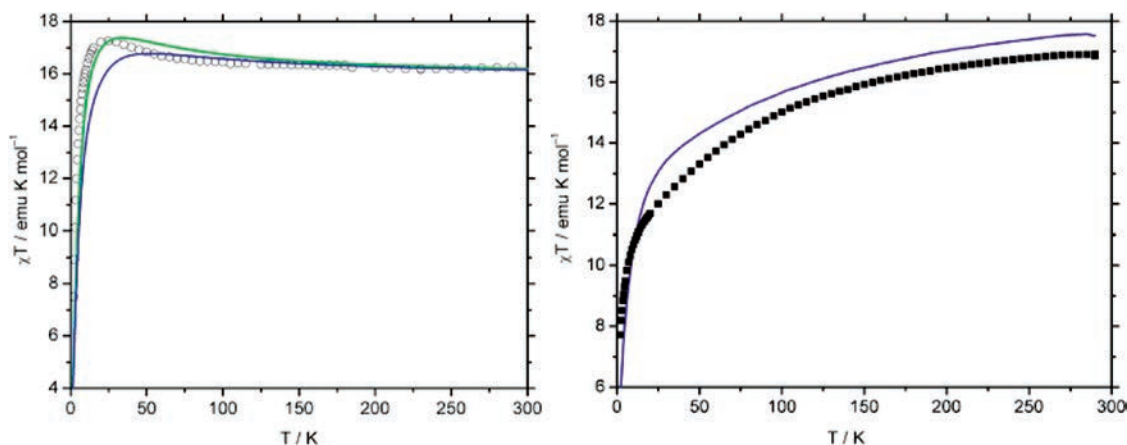


**Figure 6.** Left: Comparison of the experimental  $\chi T$  values of the  $\{\text{Ni}_{11}\text{Co}_1\}$  compound **3** (circles, 1.0 T) with the two possible site population scenarios, calculated for an approximated spin-only Heisenberg model; A (green graph), the single Co center occupies one of the six outer M positions; and B (blue graph), the Co center occupies one of the six inner M positions. Right: Comparison indicating qualitative differences between the average  $\chi T$  values of a 1:1 mixture of **1** and **2** (blue graph) with the experimental values of the  $\{\text{Ni}_6\text{Co}_6\}$  compound **4** (squares, 0.1 T).

Since classical analytical methods only can determine the bulk compositions of such compounds and single-crystal X-ray diffraction cannot unambiguously distinguish between single Ni and Co sites, probing the purity of **3** and **4**, that is, the degree of compositional deviations from the stoichiometric Ni:Co average, had to rely primarily on physical property arguments, differences in the crystal packing, and synthetic yield distributions. On the basis of the susceptibility data for **3** we observe what we could tentatively interpret as a preferred occupation of the metal positions of the inner six-membered ring by the single  $\text{Co}^{\text{II}}$  center: If in a first approximation the intramolecular exchange parameters for **2** are employed (i.e., Ni–Ni exchange is equated with Co–Co and Ni–Co exchange<sup>49</sup>) and  $\text{Co}^{\text{II}}$  is approximated as a spin-only  $s = 3/2$  center, neglecting ligand-field effects, the two resulting possible population scenarios (the Co center occupies one of the six outer sites (A) or one of the six inner sites (B)) produce different susceptibility curves (Figure 6), whereby the experimental curve for **3** closely matches the curve for scenario A. Likewise, if compound **4** were to actually consist of a 1:1 mixture of  $\{\text{Ni}_{12}\}$  and  $\{\text{Co}_{12}\}$  clusters, the resulting magnetic susceptibility data would equate to the average of the corresponding individual values for  $\{\text{Ni}_{12}\}$  and  $\{\text{Co}_{12}\}$ . The susceptibility curve for **4** differs

significantly from this average curve, indicating that no such mixture is present (Figure 6). However, because of the huge number of possible scenarios in the distribution of metal centers, inclusion of some  $\{\text{Ni}_5\text{Co}_7\}$  and  $\{\text{Ni}_7\text{Co}_5\}$  cannot be ruled out based on this evidence alone.

Cryospray mass spectrometry was utilized to illustrate that the intact clusters **1** and **2** were present in solution and not purely results of the crystallization process. Furthermore, the “naked” cluster cores (without *trans*-tach as a capping ligand) could be seen with the formulas: **1b**,  $[\text{Co}_{12}(\text{OCH}_3)_{12}(\text{O}_2\text{C}_2\text{H}_3)_9(\text{CO}_3)]^+$  ( $m/z = 1670.5$ ), and **2b**,  $[\text{Ni}_{12}(\text{OCH}_3)_{12}(\text{O}_2\text{C}_2\text{H}_3)_9(\text{CO}_3)]^+$  ( $m/z = 1666.5$ ), suggesting a substantial degree of stability in structure framework. The mixed metal clusters **3–8** give “naked” MS envelopes consistent with a statistical mixture of products, all centered around  $m/z = 1668.5$ . This rules out the possibility that compounds **3–8** are mixtures of compounds **1** and **2**. However, it does show that despite the observed site-preferences of the two metal ions, without capping *trans*-tach ligands and the site selection pressures associated with forming the crystal lattice, the metal ions are dispersed interchangeably over the same stable  $\{\text{M}_{12}\}$  architecture (Figure 7).

It can be seen in Figure 7 that spectra B–D match the predicted isotopic distributions only in position on the  $m/z$

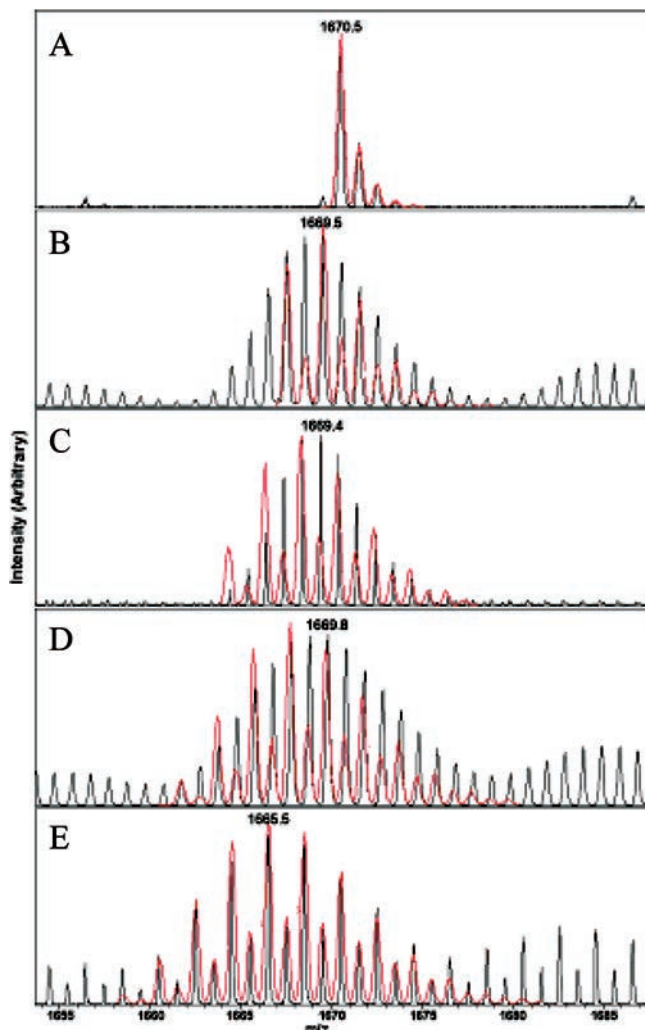


**Figure 7.** Comparison of the CSI Mass Spectra collected for the following: **A** = **1b**; **B** = {Ni<sub>3</sub>Co<sub>9</sub>}; **C** = **4b**; **D** = {Ni<sub>9</sub>Co<sub>3</sub>}; **E** = **2b**. Black spectra are the experimentally collected, and the red spectra are the predicted isotopic envelopes where **A** = [Co<sub>12</sub>(OCH<sub>3</sub>)<sub>12</sub>(O<sub>2</sub>C<sub>2</sub>H<sub>3</sub>)<sub>9</sub>(CO<sub>3</sub>)]<sup>+</sup>; **B** = [Ni<sub>3</sub>Co<sub>9</sub>(OCH<sub>3</sub>)<sub>12</sub>(O<sub>2</sub>C<sub>2</sub>H<sub>3</sub>)<sub>9</sub>(CO<sub>3</sub>)]<sup>+</sup>; **C** = [Ni<sub>6</sub>Co<sub>6</sub>(OCH<sub>3</sub>)<sub>12</sub>(O<sub>2</sub>C<sub>2</sub>H<sub>3</sub>)<sub>9</sub>(CO<sub>3</sub>)]<sup>+</sup>; **D** = [Ni<sub>9</sub>Co<sub>3</sub>(OCH<sub>3</sub>)<sub>12</sub>(O<sub>2</sub>C<sub>2</sub>H<sub>3</sub>)<sub>9</sub>(CO<sub>3</sub>)]<sup>+</sup>; **E** = [Ni<sub>12</sub>(OCH<sub>3</sub>)<sub>12</sub>(O<sub>2</sub>C<sub>2</sub>H<sub>3</sub>)<sub>9</sub>(CO<sub>3</sub>)]<sup>+</sup>.

scale, not in envelope pattern. Conversely, a statistical mixture of cluster compositions gives an approximately Gaussian distribution of peaks, similar to spectra B–D, and indeed even in the case of compound **3** where a metal ratio

of 11:1 is used (see Experimental Section). This illustrates the interchangeability between metal centers in solution, where the capping *trans*-tach ligands are disassociated from the cluster core. Compounds **1** and **2** are perfectly matched by their predicted isotopic envelopes, while simple averaging of the envelopes for **1** and **2** does not account for spectra B–D, indicating that mixed cluster cores are formed in solution.

Fragmentation studies further illustrate the mixed nature of the clusters in solution. When the cluster core peak of **2** is fragmented under cryospray conditions, using a collision energy of 50 eV/z, one of the dominating fragments is a {Ni<sub>2</sub>} unit with the formula [Ni<sub>2</sub>(CH<sub>3</sub>O)<sub>2</sub>(*trans*-tach)<sub>2</sub>(H<sub>2</sub>O)<sub>3</sub>-HCO<sub>3</sub>]<sup>+</sup>. Similar studies with **4** give a corresponding peak, with a different isotopic envelope pattern, representative of a probability distribution ({Ni<sub>2</sub>}:{NiCo}:{Co<sub>2</sub>}) of 1:2:1 (see Experimental Section).

In conclusion, the assembly and characterization of a series of isostructural {Ni<sub>12-n</sub>Co<sub>n</sub>} clusters ( $n = 0, 1, \dots, 12$ ) is achieved via the use bridging carboxylate and hydroxy/methoxy ligands, as well as templating carbonate ligands, in conjunction with bulky, terminating *trans*-tach groups. In the presented series of clusters, *trans*-tach ligands decorate the outer parts of the cubane fragments through *bis*-chelation via the *cis*-amino groups while the protonated *trans*-amino group acts as a hydrogen bond donor in a supramolecular hydrogen-bonded array in the crystalline state. As the required reaction parameters for the synthesis of these mixed-metal coordination clusters are not confined to the stoichiometric Ni:Co reactant ratio, but also rely upon the acidity of the solution, crystallization of very pure mixed-metal species appears possible, especially at the outer edges of the series. Mass spectrometry illustrates the mixed nature of the clusters in solution, whereas magnetic studies have indicated the possibility of site specificity of the constituents once locked in the crystalline lattice, where these additional site-selection pressures exist.

**Acknowledgment.** The authors wish to thank the EPSRC and the University of Glasgow for funding.

IC802197U